DEUTSCHES ELEKTRONEN-SYNCHROTRON DESY

DESY SR 85-11
October 1985

NIKOS - A SYSTEM FOR NON-INVASIVE EXAMINATION OF CORONARY ARTERIES BY MEANS OF DIGITAL SUBTRACTION ANGIOGRAPHY WITH SYNCHROTRON RADIATION

by

W.-R. Dix

Deutsches Elektronen-Synchrotron DESY, Hamburg

K. Engelke, C.-C. Glüer, C.P. Höppner

II. Inst. f. Experimentalphysik, Universität Hamburg

W. Graeff, K.-H. Stellmaschek, T. Wroblewski

Hamburger Synchrotronstrahlungslabor HASYLAB at DESY

W. Bleifeld, K.H. Höhne, W. Kupper

Universitäts-Krankenhaus Eppendorf, Hamburg

ISSN 0723-7979

NOTKESTRASSE 85 · 2 HAMBURG 52

To be sure that your preprints are promptly included in the HIGH ENERGY PHYSICS INDEX, send them to the following address (if possible by air mail):

DESY
Bibliothek
Notkestrasse 85
2 Hamburg 52
Germany

DESY SR 85-11
October 1985

ISSN 0723-7979

NIKOS - A SYSTEM FOR NON-INVASIVE EXAMINATION OF CORONARY ARTERIES BY MEANS OF DIGITAL SUBTRACTION ANGIOGRAPHY WITH SYNCHROTRON RADIATION

W.-R. Dix (a)
K. Engelke (b)
C.-C. Glüer (b)
W. Graeff (c)
C.P. Höppner (b)
K.-H. Stellmaschek (c)
T. Wroblewski (c)
W. Bleifeld (d)
K.H. Höhne (d)
W. Kupper (d)

(a) Deutsches Elektronen-Synchrotron DESY, Hamburg.
(b) II. Institut für Experimentalphysik, Universität Hamburg.
(c) Hamburger Synchrotronstrahlungslabor HASYLAB at DESY, Hamburg.
(d) Universitäts- Krankenhaus Eppendorf, Hamburg.

ABSTRACT

Two entirely different schemes for K-edge subtraction angiography have been tested. The first system, consisting of a fast switching monochromator and an image-converter / TV-camera detector, proved to have several disadvantages for this purpose. Subsequently a second system (NIKOS I), consisting of a focussing double beam monochromator and an intensified photodiode detector, has been designed. Results are available from a preliminary version of NIKOS and these compare favourably with respect to the first system for images of excised pig hearts.

submitted to Nucl. Instr. & Meth.

CONTENTS

1.0 INTRODUCTION

Coronary heart disease and its most serious complication, the myocardial infarction, is the leading cause of death in the industrial world. The reason for an acute myocardial infarction is almost always an acute thrombotic occlusion of a coronary artery at the site of a preexistent stenosis.

If it would be possible to detect coronary artery stenoses prior to a myocardial infarction, interventions such as a by-pass-operation or a percutaneous transluminal coronary artery dilatation could salvage the myocardium. Today the only possibility to visualize the anatomical situation of the coronary arteries is selective coronary angiography. During this invasive procedure a contrast agent (370 mg/ml iodine) is injected into the arteries via a catheter. This way high contrast images are obtained with conventional X-ray generators and standard image intensifiers. On the other hand the procedure carries significant risk to the patient with respect to mortality (0.07 to 0.23%) and morbidity (1.2 to 2.2%). These considerable risks do not allow selective coronary angiography to be used as a screening test.

For routine investigations a non-invasive method of coronary angiography without using a catheter is necessary. During such a procedure the contrast agent is introduced into a peripheral vein. Before entering the coronary arteries it is diluted in the central circulation system. Hence, compared to the invasive application, the iodine concentration is much less. However, it is not possible to get sufficiently good images of the anatomical situation with conventional radiologic equipment.

During the last few years, digital subtraction angiography (DSA) has become a powerful method for non-invasive investigations [1], [2], [3]. In the time-subtraction-mode images are produced before and after application of the contrast agent, followed by their digital subtraction. In the resulting image the visibility of the contrast agent is strongly enhanced because unwanted soft tissue and bone contrast is suppressed. However, any moving structure leads to artefacts. So, DSA in time-subtraction-mode is acceptable for most vascular regions except the heart, if arteries of at least 1 mm diameter are to be imaged. Even more complex systems that take the two images at equivalent phases of the heart cycle (ECG - trigger) are limited to several millimeter resolution due to the nonperiodic motion of the heart [4].

These difficulties can be overcome with a different mode of DSA - the energy-subtraction-mode. In this mode the two images for subtraction are produced in the presence of iodine using two different energies E_1 and

E_2 respectively. These lie below and above the K-absorption-edge of iodine (33.16 keV). The difference in iodine contrast which is essential for DSA is caused by the abrupt change of the iodine absorption coefficient at the K-edge. Using radiation with a small energy bandwidth (typically 100 eV) both soft tissue and bone contrast are suppressed in the subtracted image. Only synchrotron radiation offers enough intensity in such a small bandwidth to take the images fast enough. With broadband dual energy techniques [5] using conventional X-ray sources residual contrast of either bone or soft tissue is still visible due to the monotonous energy dependence of the corresponding absorption coefficients.

A system suited for the imaging of coronary arteries with non-invasive DSA in energy-subtraction-mode should fulfill the following conditions:

Arteries down to 1 mm diameter should be visible leading to a matrix size of 256×256 pixels with 0.5 mm pitch.

Intravenous application of iodine into a brachial vein (10 ml contrast agent within 1 sec) results in an iodine concentration of 10 mg/ml in the coronary arteries corresponding to 1 mg/cm^2 in arteries of 1 mm diameter giving a 3%-signal in the subtracted image. Aiming at a signal-to-noise ratio (SNR) of at least 3, noise has to be limited to 1%.

The two images must be taken within the same heart cycle at a phase of minimum motion of the heart (typically within 200 ms) in order to avoid motion artefacts and strong image distortions.

The 1%-noise requirement leads to a minimum flux of 1.4×10^4 detected photons per pixel at each energy. Assuming the time requirements mentioned above and transmission through 20 cm of soft tissue this corresponds to an intensity ahead of the patient of about 5×10^{10} phot/mm^2 s. At existing synchrotron radiation centres this intensity is available only in wiggler-beam-lines.

At present, experiments on coronary angiography are carried out in the facilities at Stanford [6],[7], Tsukuba [8], Novosibirsk [9],[10] and Hamburg. At Hasylab in Hamburg we have started by testing an energy switching monochromator and a conventional area detector. Results of these experiments including images of excised pig hearts, which are reported below, led to the development of the NIKOS system. This system, as well as tests on individual components, is described in detail.

2.0 INITIAL APPROACH: AN IMAGE CONVERTER AREA DETECTOR WITH A FAST SWITCHING MONOCHROMATOR

In order to make full use of the vertical spread of the synchrotron radiation beam which is of the order of 0.2 mrad (corresponding to a few mm height at the detector) either focussing optics or an area detector is needed. One type of detector that should be able to cope with the high incident flux is an integrated X-ray image intensifier video chain where the intensity is integrated as an electrical charge on the target of the video tube. An attractive advantage of these technically well developed systems is their widespread use in radiology. Hence it seemed to be reasonable to test such a detector for synchrotron radiation coronary angiography.

2.1 EXPERIMENTAL SETUP.

All our experiments on angiography using synchrotron radiation have been performed at the topography station at Hasylab. This station is at a distance of 34 m from the source and receives synchrotron radiation from a bending magnet of the electron storage ring DORIS. During most of the experiments DORIS was running between 5.0 and 5.3 GeV electron energy and 20 - 40 mA current. Under these conditions the incident photon flux at 33 keV is about 10^8 phot/mm^2·eV·s. The maximum horizontal beam aperture is 50 mm. In the following the components of the experimental setup (Figure 1) are described in more detail.

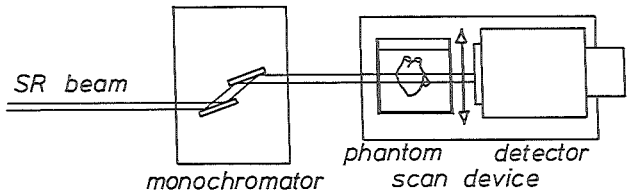

Figure 1. Schematic diagram of the experimental setup for non-invasive angiography.

2.1.1 The fast switching monochromator.

Due to the limited beam height a full illumination of the heart is possible only via widening the beam cross section by the use of appropriate crystal cuts. In this case, specific problems arise from the large crystal size. As the local intensity is decreased, a more powerful source is needed. Above all, the image contrast is strongly reduced by scatter in the patient as discussed below.

Alternatively the region of the heart can be scanned in a vertical direction. Although from the medical point of view it would be desirable to move the beam and keep the patient at rest, the necessary mechanical design would be so complex that we prefer to move the patient through the beam until the method has been fully evaluated.

Both images (E_1 and E_2) have to be recorded during one heart cycle in a single scan. So the images have to be taken in horizontal slices and the energy must be switched rapidly in between. This requires a monochromator which can be moved between two different angular positions in a very short time.

We have chosen a double crystal monochromator as its outgoing beam stays practically stationary for small rotations of the system. The two reflecting parts of the monochromator have to remain parallel within a few seconds of arc.

In principle, a channel cut crystal would provide the necessary stability especially at fast rotational steps. But the well-known disadvantages of the monolithic version, such as bad harmonic rejection and contamination with unwanted reflections, led us to the installation of a separate function monochromator which consists of two independent crystals.

The design of the monochromator [11] (Figure 2 on page 5) was mainly determined by the demand for a compact rigid mounting of the crystals with a low moment of inertia. Therefore the crystals are mounted inside a rectangular frame where only one positioning element is integrated. This element, a piezoceramic, controls the parallel setting of the two crystals. The frame itself is held by two torsional spring pivots with negligible friction. The angular position of this frame with respect to the incident beam defines the transmitted energy and is adjusted by a loudspeaker coil. A dc bias sets the monochromator to the K-edge position, whereas the ac component of the coil input wobbles the monochromator around its center position at frequencies of several hundred Hertz. Its amplitude can be chosen in such a way that the transition time from one energy to the other is only 10 - 15 % of the full cycle. For monochromator crystals, two

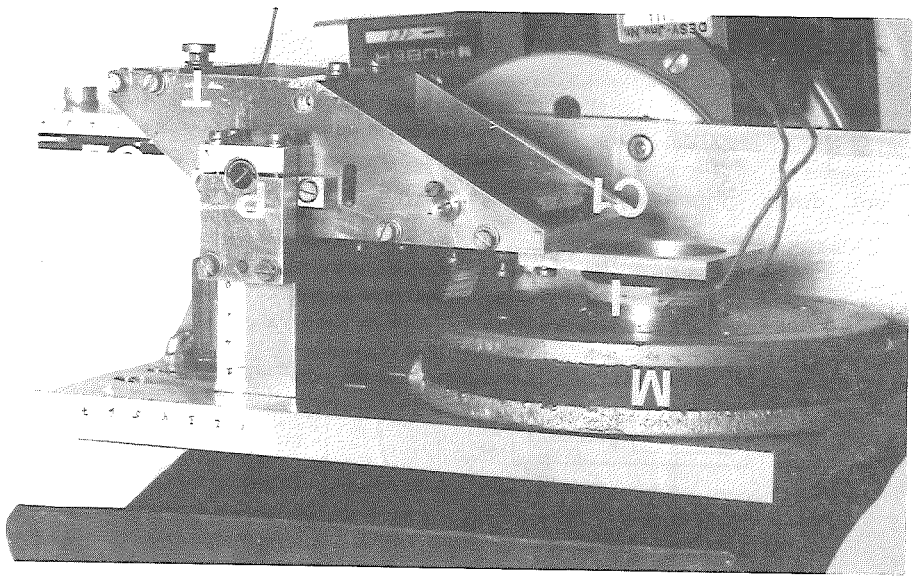

Figure 2. The fast switching monochromator for switch rates up to 100 Hz: Piezoelectric translator (T) and torsional pivots (P) for parallel setting of the two crystals (C1 and C2). The induction coil (I) oscillates in the sinusoidally changing field of the loudspeaker magnet (M) thereby changing the transmitted energy.

plates of germanium were used, 60 mm wide and 80 mm long. For the Ge 220 reflection the Bragg angle at the iodine K-edge is $\Theta = 5.36°$ and the intrinsic bandwidth is $\Delta E = 4.8$ eV. In this case an energy spacing $E_2 - E_1 = 100$ eV corresponds to a difference in Bragg angle $\Delta\Theta = 0.016°$. Harmonic rejection was accomplished, as usual, by a slight missetting of the crystal plates.

2.1.2 The scanning device

To avoid artefacts in the subtracted image, a very uniform motion of the scanning device is required. In addition it must be able to carry a heavy load. After investigation of various systems we finally ordered a mechanically driven table from a firm specialized in linear driving systems [1]. Its

[1] Fa. Uhing, Kiel, FRG.

central part is a hardened and polished driving shaft which rotates at constant speed. The moving table is clamped to this shaft by pairs of ball bearings. When the orientation of their axis of rotation is inclined with respect to the shaft the ball bearings start to move along the shaft. The speed is controlled by the angle which can be changed by an external steering shaft. Thus the motion of the table can be varied continuously although the driving motor rotates at constant speed.

This scanning device can carry up to 100 kg net load and move up to 40 cm with a velocity of 60 cm/s. The actual position of the table during the scan is recorded by a train of electric pulses which are generated in an incremental linear transducer [2].

2.1.3 The X-ray detector system

The detector used, consisted of a TV camera optically coupled by lenses to an X-ray image converter[3] . Its characteristics are a 100 mg/cm^2 CsI input phosphor screen, 16 cm input screen diameter, a P 20 output phosphor and a standard 50 Hz interlaced BAS video output. Horizontal and vertical pixel pitch were 0.5 mm and 0.33 mm respectively. The TV camera has been equipped with either a Saticon or a Hivicon tube that mainly differ in temporal response. The Saticon shows an afterglow of 15% after 60 ms, the Hivicon of 50% after 100 ms.

2.1.4 The image processing system

The image processing system included a computer (PDP 11/34) and a commercially available digitizer (MVD from VTE). The BAS-signal of the TV-camera was digitized and stored in real time (sampling rate 10 MHz). Two images (512 × 512 × 8 bit) can be stored. The software for the system is written in PROFI-11 [12], a language especially developed for image processing.

[2] Heidenhain LIDA 19
[3] Siemens SIRECON-2 BV

2.2 RESULTS AND DISCUSSION

With the setup described above two major questions were to be answered:

- Does the monochromator perform properly at the required high frequencies?
- Is an image-converter area detector a well-suited detector system for coronary angiography with intravenous contrast injection?

2.2.1 Monochromator tests

The absolute photon flux behind the monochromator was measured by a NaI detector and compared to theoretical calculations. Although beam optical parameters have been included, only 80 % of the calculated values were reached. During this measurement a small pinhole was used to avoid detector saturation and heating effects.

The resonance frequency of the movable part of the monochromator has been measured to be 8.9 Hz. Above a 70 Hz driving frequency, which is well above the resonance frequency, the measured phase shift between driving voltage and rotational oscillation stays practically constant at 180°.

The most interesting parameter was the upper frequency limit of the monochromator. The reflectivity averaged over an oscillation period was measured for different frequencies and amplitudes. For instance, at 100 Hz and 1 V ac coil input, corresponding to an energy spacing $E_2 - E_1 \sim 400$ eV, 80 % of the reflectivity at rest is still attainable. At higher frequencies the reflectivity drops rapidly.

The reason for this drop is a phase shift between the individual oscillations of the two crystals, as detected in a phase resolved measurement. The resulting deviation from parallel setting causes oscillations in the momentary reflectivity, e.g. between 60 % and 100% at 100 Hz, 1V. A more rigid mounting of the crystals, on the other hand, would cause additional problems due to heat induced strains.

The dead time between the recordings of different energy is determined by the time the K-edge is crossed. Taking into account the intrinsic energy bandwidth of the reflection and the energy spread caused by the vertical beam divergence, an energy gap of 150 eV around the K-edge is necessary for optimum contrast. For instance at 100 Hz, 1 Volt, this gap is passed in 1 ms leaving 80 % of the full cycle of 10 ms for exposure. Shortening of

this transition time by larger amplitudes decreases the iodine contrast: at $E_2 - E_1 \sim 1$ keV a loss of 23 % in iodine contrast was measured.

It is concluded that the fast switching monochromator can be operated up to frequencies of 100 - 150 Hz without significant loss of performance. But frequencies up to 1 kHz as they are required for the acquisition of images within a heart cycle are not obtainable with this device without major improvements.

2.2.2 Detector tests

The detector system is used and optimized for a variety of radiological applications in the photon energy range of 40 to 80 keV. Since we wanted to use it under non-typical conditions, concerning photon energy, time resolution and noise level, and since few data was available, the detector system was tested with respect to the parameters listed below.

Spatial resolution. The shadow of a tungsten wire of 1.5mm diameter was imaged. In the central pixel we still got around 10% intensity and the profile was smeared out to five pixels (2.5 mm) on a 75% signal level and to seven pixels (3.5 mm) on a 90% level.

Response. The intensity profile of the beam behind an aluminium wedge was measured with a NaI-reference detector giving an intensity variation along the wedge of a factor of 40. Afterwards, the same profile was imaged with the Sirecon detector. Its responsivity could be varied by inserting diaphragms of different aperture between the image converter and the TV camera. The BAS-signal was digitized with 8 bit resolution. Dark current accounted for about 12 to 16 greylevels with the internal dark current correction of the Sirecon being disabled. Using the Saticon tube the response was quite linear up to 220 greylevels provided up to 10^3 photons/pixel were recorded. Increasing the flux up to 10^4 photons/pixel (this being the required amount) led to saturation above about 200 greylevels.

Additional problems would arise if we collected these photons in an integration time of 1 ms. Siemens specifies a linear response of the image converter up to 100 mR/s corresponding to approximately $5 \cdot 10^3$ photons/pixel·ms. Aiming at a noise level of about 1% we will have to detect at least $1.4 \cdot 10^4$ photons/pixel·ms. Moreover a much higher intensity has to be detected in those areas of the image where the beam passes mostly through lung tissue. Resulting intensities of 10^5 photons/pixel·ms are far beyond the saturation level of currently available medical image converter systems.

Noise. Every response curve measurement was repeated 50 times at intervals between measurements of less than a second. From this we calculated statistical fluctuations of response as a function of registered photon flux. The lower noise limit was determined to be 2% of the signal. Due to afterglow the information is smeared out over several readout cycles. Therefore, with continuous exposure the noise is reduced as compared to a single frame exposure. Hence for the single frame exposure in intravenous angiography, noise would be more than 2% whilst only 1% is tolerable.

K-edge implications. Due to the presence of iodine in the input phosphor screen one gets a decrease in yield for X-ray photons with energies just below the iodine K-edge with respect to those just above the edge. We measured a decrease of 34%.

Below the K-edge the input phosphor only absorbs 50% of the incoming radiation. This means that only 50% of all X-ray photons which contribute to the dose give image information.

Dynamic range. A simple definition of the dynamic range as

$$D = \frac{\text{maximum output signal}}{\text{noise at max. output signal}}$$

is not adequate for subtraction angiography because the absolute noise level is smaller at lower signals. Looking for a figure of merit that illustrates the range of detectable signals an appropriate definition of dynamic range would be

$$D^* = \frac{\text{maximum output signal}}{\text{noise at signal levels with SNR=3}}$$

For continuous exposure the dynamic range was measured to be 85. In our application it would be reduced by the K-edge yield variation as well as the noise enhancement for single frame exposure to less than 30.

Scattered radiation. The benefit of imaging several lines at a time with an area detector is that for a given total exposure time of 200 ms (heart nearly at rest at the end of diastole or systole) one gets longer integration times for each line. So the demands on the storage ring's emitted X-ray intensity would be lowered. On the other hand investigations of conventional angiographic scene records taken with high time resolution revealed that integration times longer than 4-6 ms lead to motion artefacts.

Secondly the amount of detected scattered radiation increases. Measurements with several different synchrotron beam cross sections showed scatter fractions (detected scattered radiation / total detected radiation) behind a water-filled lucite cube (175 mm edge length) between 0.35% and 1.7% for beam cross sections between 3×3 mm² and 24×3 mm². Extrapolation of the measured data to a typical angiography beamsize at a storage ring which would be 100×7 mm² yields an expected scatter fraction of 8%. A larger beam width would increase the scatter fraction even further. This is indicated by experiments on X-ray tubes where a change of field width from 100×100 mm² to 350×350 mm² resulted in a variation of scatter fraction from 47% to 63% [13]. With increasing scatter-fraction the SNR of the subtracted image gets worse.

Summarizing the results of our measurements one can list the following disadvantages of a conventional image converter area detector for our special application:

1. low dynamic range,
2. long afterglow,
3. count rate limitations,
4. high scatter fraction,
5. low X-ray absorption below the iodine K-edge.

Point 2 could be overcome by separating the light output originating from different energies either by means of a color TV camera [8] or by optical beam splitters. The problems related to point 3 and especially Point 5 could be solved only by major changes in the converter (decreasing the gain and exchanging the input phosphor). Presumably also the output phosphor of the converter had to be exchanged since P 20 is not fast enough [4].

The major reason for testing the converter/TV camera system was its current widespread use and commercial availability. But considering all of the modifications that would have to be realized, it turned out that a lot of development would have to be done. In any case the disadvantage of a high scatter fraction makes it questionable that even after sophisticated improvements an area detector system would be well suited for intravenous angiography. So it is more promising to develop a new line scan detector system that is designed to satisfy our specific demands.

---

[4] 16.4% afterglow after 1 ms (Philips technical data for an image converter equipped with a P 20 output phosphor)

2.2.3 Scans of excised pig hearts

To test and demonstrate the features of the converter/TV camera system we imaged excised pig hearts. The coronaries were filled with a barium compound. The chosen concentration should yield a contrast equivalent to the iodine concentration expected with humans. Because of the limited width of the beam (5 cm) the images could not be taken in a single scan. For each energy four partly overlapping scans had to be taken to cover the whole area of the heart. The long afterglow of the TV tube required a fixed mounting of the detector with respect to the object. In addition the energy could not be switched within a scan. So heart and detector were mounted on the scanning device that moved with a uniform velocity of 5 cm/s.

During each scan the subsequent images of the TV-camera (rate 50 Hz) were digitized, corrected for background and added in real time. Each scan pair (two energies) was subtracted logarithmically and afterwards all

Figure 3. **Subtracted image of an excised pig heart taken with the image-converter/Saticon detector system: The coronaries are filled with a paste containing 17.4 mg/ml Ba (resulting in the same contrast as 14 mg/ml iodine). Scan speed 5 cm/s. Due to the low dynamic range bone contrast is still visible as white noisy background.**

four resulting subtracted images were composed to form the subtracted heart image of Figure 3.

It is obvious that the image quality suffers from the low dynamic range of the detector. So one realizes that the bone contrast does not cancel out completely but results in a very noisy background. Additional intensity variations from line to line can be seen that are due to the lacking synchronization of camera and scanning device as well as to a missing beam intensity monitor.

3.0 NIKOS I: A DOUBLE LINE SCAN SYSTEM WITH A STATIONARY MONOCHROMATOR.

3.1 EXPERIMENTAL SETUP

Experience with the experiments described above led to a completely new design of both the monochromator and the detector. In order to avoid all the problems with oscillating crystals or fast moving shutters we designed the double line scan system NIKOS I (Nicht - invasive Koronarangiographie mit Synchrotronstrahlung) where only the patient is moved and all other components are stationary. The basic idea is to provide two closely spaced parallel beams with energies E_1 and E_2 and register these beams simultaneously when scanning the patient. The result is a pair of images with a small time shift of a few milliseconds between the recording of corresponding lines.

3.1.1 The focussing double beam monochromator

Splitting of the incident beam into two monochromatic beams can be achieved in two different ways. In one way the upper and lower part is reflected by two independent crystals. If one omits a second reflection of the monochromatic beams as it is done with the setup at SPEAR one can even focus the two beams by bending the crystals appropriately. A disadvantage of this arrangement is its sensitivity to vertical beam oscillations as they are frequently found with existing storage rings. As the resulting intensity oscillations in both beams are in counterphase the effect is even doubled when subtracting the two images.

A more elegant way of beam splitting is illustrated in Figure 4 on page 14. The full beam cross section is transmitted twice through very thin Laue case crystals (reflecting netplanes perpendicular to the surface). This geometry has two advantages. Firstly beam oscillations do not affect the subtracted image and secondly, without any bending of the crystals, the beams are focussed onto the detector [14]. It is planned to use a Si 111 reflection in the Laue crystals and a Ge 111 reflection in the Bragg crystals. This combination has an excellent higher harmonic rejection. The difference in Bragg angle is $\Delta\Theta = 0.14°$ resulting in an angular deviation of 0.28° of the monochromatic beam from the incident beam. This provides, at a distance of 16 m from the monochromator, a sufficiently large separation of the monochromatic beams from the secondary high energy particle showers generated in the wiggler straight section to be safely stopped before reaching the patient. The small wavelength dependence of $\Delta\Theta$ allows for making the two beams E_1 and E_2 slightly convergent so that at the monochromator they are separated by 6 - 8 mm corresponding to the beam height at that place and at the detector they have a spacing of 2 mm, only.

The thickness of the Laue crystal very much affects the reflectivity due to the interference of two wavefields inside the crystal, the so called Pendellösung effect [15]. The optimum thickness for a photon energy of 33 keV is 31 μm. With such a thickness absorption can be neglected and about 70% of the Bragg case reflectivity is reached. As the beam is used twice a net gain of 40% can be achieved.

The mechanical stability of such a thin crystal is ensured by leaving a thicker frame around the thin reflecting part of the crystal. For cooling purposes the crystal is kept in a 3 mm thick flat container with thin mylar windows under flowing water.

The monochromator drive, as shown in Figure 5 on page 15, comprises two identical goniometers. Energy adjustment is done by rotating the upper part of each goniometer, carrying the two crystals, by the supporting arc segment. The second crystal is mounted on torsional spring pivots and can be adjusted with the necessary angular precision by a piezodrive. This piezodrive is also an important part of the radiation safety precautions, because in case of any malfunction of the scanning table the beam can be switched off within a millisecond by discharging the piezodrive and thus missetting the second reflecting crystal about a few seconds of arc.

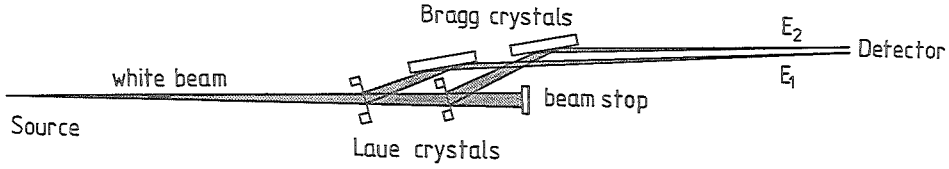

Figure 4. Schematic beam geometry of the focussing double beam monochromator: Focussing is achieved by the combination of flat Laue and Bragg case crystals. The energy of the beams can be adjusted independently.

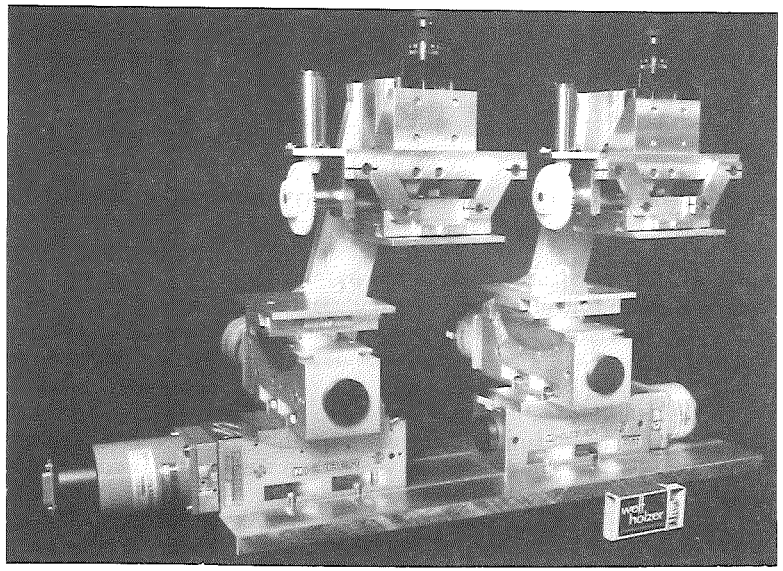

Figure 5. The double beam monochromator: It consists of two identical goniometers. Crystals are not mounted.

3.1.2 The intensified photodiode detector

The general design of the detector is shown in Figure 6 on page 16. It consists of a phosphor screen, an image-intensifier and a photodiode-array all these components being coupled by means of special fibre optics. The two X-ray beams generated by the monochromator are converted into visible light by means of a phosphor screen. This screen consists of two rows of luminescent material, one for each X-ray beam spaced by 1.5 mm. The dimensions of each row are 63.5×0.5 mm² thus constituting 127 pixels 0.5×0.5 mm each. The luminescent material either could be a powder phosphor or a scintillating crystal.

The optical light output of each phosphor pixel is transferred to an image-intensifier by means of a glass fibre bundle. This bundle consists of about 250 single glass fibres of 30μm diameter glued together to a quadratical cross-section of 0.5×0.5 mm² at the phosphor side and a circular cross-section of 0.7 mm diameter at the image-intensifier side.

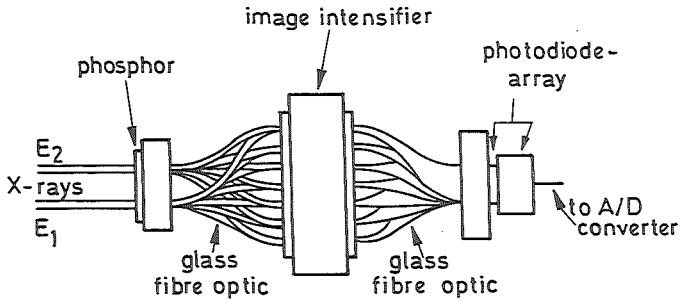

Figure 6. Schematic layout of the double line scan detector: At the input face two lines of 127 pixels each (63.5 mm total length) are fibre-optically coupled to an image-intensifier of 25 mm diameter. The output of the image-intensifier again is coupled to the entrance window of a photodiode array.

A small fraction of each of the two monochromatic beams is stopped by two monitor-phosphors to detect the beam intensity in front of the patient. They are coupled to the image-intensifier by two additional fibre bundles thus also monitoring the gain of the image-intensifier.

To enhance the light level of the phosphor screen to the needed intensity level for the photodiodes, an image-intensifier having a gain factor of about 100 along with little image distortion and sufficient resolution is required. We chose a double stage proximity focused image-intensifier having zero distortion [5], the required gain factor and a limiting resolution of 25 line pairs / mm at 3-5 % contrast (30-40 % at 10 line pairs / mm). To get a minimum crosstalk the 256 incoming fibre bundles are distributed over the whole active input area (25 mm diameter) of the image-intensifier aiming at maximum distance between individual bundles. A center to center spacing of 1.3 mm is attainable. The resulting distance between adjacent bundles of ≧0.6 mm should reduce crosstalk to an acceptable level.

[5] Proxitronic Proxifier BV 2533 MX 35

A second set of 256 glass fibre bundles is positioned at the output face of the image-intensifier to collect the intensified input signals. In this way every bundle of the second set just carries the information from one phosphor pixel. Whereas the input cross-section of these second bundles again is circular (0.7 mm diameter) at the image-intensifier output face, their output end is formed to give a cross-section of 0.1×2.5 mm^2 to match the photodiode sizes.

The photodiode-array is a Reticon RL 1024 SF chip consisting of 1024 photodiodes each having a 0.025×2.5 mm^2 input area. The second fibre bundles closely packed side by side to form a single line are coupled to the Reticon chip. In this way every bundle covers four photodiodes. Thus the fibres not only serve to couple the individual components of the detector but also produce a cross-section-transformation for each pixel from 0.5×0.5 mm^2 to 0.1×2.5 mm^2. Since no tapering is necessary there are no losses of aperture and the light intensity incident on each photodiode should be enhanced by a factor of five.

As far as the electronic readout is concerned, we started by using Reticon's standard evaluation circuit for the S-series arrays. It was modified in the following way :

1. Due to the outer shape of our fibre optic the Reticon chip had to be removed from its socket on the evaluation circuit and put on an external socket about 25 cm away.

2. The internal readout trigger was replaced by an external one. In our setup a Heidenhain position sensor monitors the movement of the scanning device. Every 0.5 mm a signal is sent as an external trigger to start a readout of one Reticon line. Additional modifications have been made to synchronize this pulse to the Reticon clock.

3. An integrator/amplifier stage was added to the sequential analog output port of the Reticon evaluation circuit to integrate the signals of each four diodes that correspond to the same input phosphor pixel. Also the signal is amplified to an appropriate level for the following 12 bit, 0.5 MHz ADC[6] .

4. All TTL ICs of the evaluation circuit have been exchanged by modern QMOS ICs.

[6] Datel ADC - 817

3.1.3 The image processing system

Two computers connected via PADAC are installed. A PDP 11/40 is used for the control of the complete system (CAMAC). In the PDP 11/34 the PROFI image processing system is running. Using the DESY-online-system this computer is connected to the DESY computing center to make available additional storage and computing power.

To get images the object is moved through the beam with a speed of 6 cm/sec. The detector is fixed. The incoming data from the detector are first stored in a PADAC-buffer. The data can be stored with a rate of 0.5×10^6 pixels/sec (1 pixel corresponds to 12 bit). After finishing the scans the image (256×256 pixels) is transferred into the MVD-buffer connected to the PDP 11/34.

To correct for beam fluctuations and unstabilities of the scanning device each line of the image is corrected corresponding the monitor-signal. After logarithmic subtraction of the two scan-images (E_1 and E_2) the resulting "subtracted scans" are composed to get the final images shown in Figure 9 on page 22. Each image is composed of 6 overlapping scans. The width of the scans was 2.5 cm.

3.2 FIRST RESULTS

Experiments to test the individual components of the detector as well as their combination in a preliminary version were carried out. In this version X-ray input phosphor screens were directly coupled to the input fibre optic faceplate of the image-intensifier. The output fibre of the second image-intensifier was coupled to the Reticon by means of a rigid image conduit. The Reticon was operated with an integration time of 10ms.

Important parameters to characterize the detector system are afterglow, absorption fraction, conversion efficiency with respect to the input characteristic of the image-intensifier, noise, dynamic range and resolution.

Afterglow of different phosphors was measured by chopped irradiation with synchrotron radiation. The decay of the emitted light flux generated by 1ms X-ray pulses was detected with a fast photomultiplier. A LED on the chopper triggered a MCA operated in a multichannel scaling mode. Results are presented in Figure 7 on page 19. The curve of the $CdWO_4$ crystal was taken as a reference. Here the leading and the trailing edge are mainly determined by the chopper slit. The shortest afterglow of a powder phosphor was obtained for P36 which is (Zn,Cd)S:Ag,Ni. As compared to the values for the Saticon and the Hivicon tubes mentioned above, the

afterglow times of Gd_2O_2S: Tb and Y_2O_2S: Eu are much shorter, too. But for single line integration times of about 1 ms it is obvious that in each line one has to eliminate the afterglow fraction of the two foregoing integration periods. This image processing introduces additional noise because the information for one pixel is spread over several integration times.
Meanwhile we obtained faster versions both for Gd_2O_2S: Tb and Y_2O_2S: Eu but detailed afterglow measurements on these two phosphors have not yet been carried out.

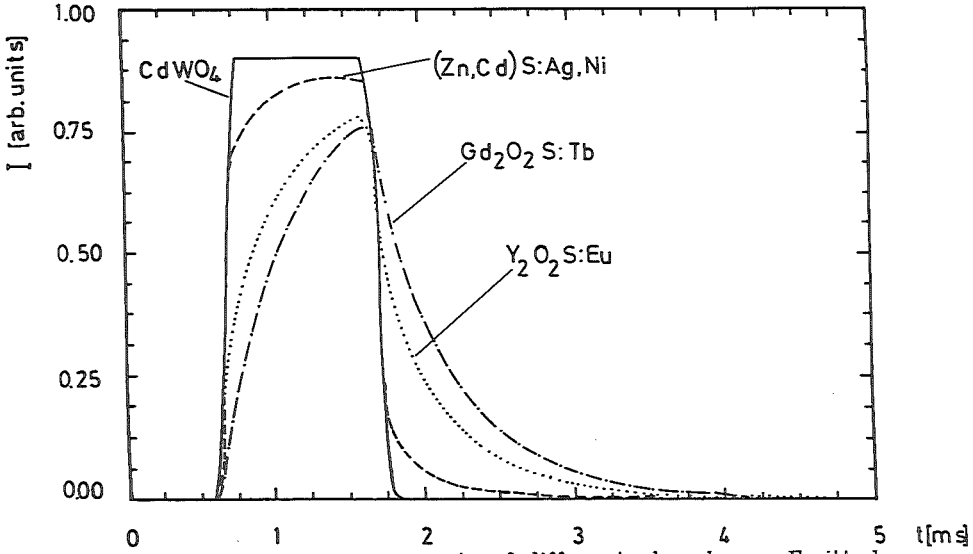

Figure 7. Afterglow measurements of different phosphors: Emitted light intensity I as a function of time t. $CdWO_4$ which has a very short afterglow served as a reference to show the incident X-ray intensity as a function of time.

The image-intensifier was ordered with an extra fast output screen the afterglow of which was specified to be less than 1% after 200 ns. The maximum clock frequency of the Reticon chip is 5 MHz but one is limited to 300 kHz when using Reticon's standard evaluation circuit. Additionally we observed an 8% residual signal in the subsequent readout. This is due to a limitation in the recharging reset current and should presumably be overcome by external reset transistors. Modifications of the evaluation circuit to increase the frequency are currently being tested.

Conversion efficiency and emission spectra of phosphors can be found in the literature [16], [17]. We measured the relative efficiency of combined phosphor/image-intensifier systems. Values of light output of the image-intensifier per absorbed X-ray quanta with respect to Gd_2O_2S: Tb measured at the I K-edge are as follows :

Gd_2O_2S: Tb	100%
Gd_2O_2S: Tb(fast)	55%
Y_2O_2S: Eu	32%
Y_2O_2S: Eu(fast)	32%
(Zn,Cd)S: Ag,Ni	18%

Due to self-absorption this conversion efficiency decreases with increasing mass per unit area.

Noise. Two major components determine the noise level in angiography examinations : statistical quantum noise and detector noise. To reach the quantum limit as many X-ray quanta as possible should be absorbed in the phosphor. Since always several light photons are generated by one absorbed X-ray photon light losses are less crucial.

Reticon noise as a function of illumination is plotted in Figure 8 on page 21. The noise of the image-intensifier is three orders of magnitude lower. Thus the phosphor is the principal target for optimization with respect to thickness and preparation method.

Dynamic range. With the definition of D*, from Figure 8 on page 21 one can determine the dynamic range of the Reticon to be 2500 in the present set-up. Modifications of the evaluation circuit should enhance this level.

Resolution of the phosphor drops with increasing mass per unit area. To circumvent this, it should be possible to put a very thin light absorbing wall between adjacent input pixels. By this means cross talk of visible light would be reduced. Crystals can be cut in small blocks (one for every pixel), coated on five faces with a reflecting material and glued with their sixth face side by side on top of the fibre.

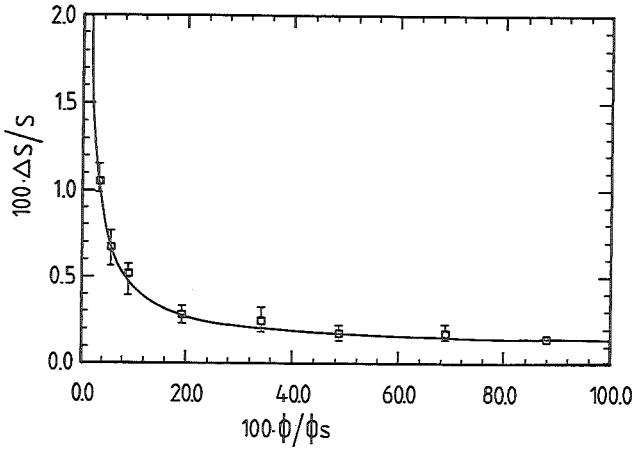

Figure 8. Reticon noise: Relative noise ΔS / S of the Reticon output signal S as a function of the incident light flux Φ emitted from LEDs. Absolute noise rises with increasing incident flux levels. The critical value of 1% detector noise (see text) is reached at 4% of the saturation flux Φ_S.

Images of excised pig hearts. With the new detector system working in this preliminary version we again imaged the excised pig hearts. Figure 9 on page 22 shows images above and below the K-edge as well as the subtracted image. Because of the enhanced dynamic range of the new system consequently all air bubbles disappear on the subtracted image. One of the two bones also vanishes whereas a contrast of the edges of the second bone remains. But its characteristic feature, one edge being imaged as a black line and the other as a white line, leads to the conclusion that the bone must have moved between the scans of different energy. In the final setup corresponding lines are imaged within 5 ms. So this kind of artefact should not appear then.

Looking at the detector readout the exposure of every photodiode is delayed by 10 μs with respect to the preceding one. So the longer the distance of a photodiode from the beginning of the line, where the monitor signal is recorded, the larger is the time difference between the recording of the monitor signal and the particular diode. So beam fluctuations on a scale comparable with the readout time cannot be corrected. This uncorrected intensity variation within a line is strongly enhanced in the subtracted image. The envisaged decrease of the readout time by a factor of ten should reduce these artefacts.

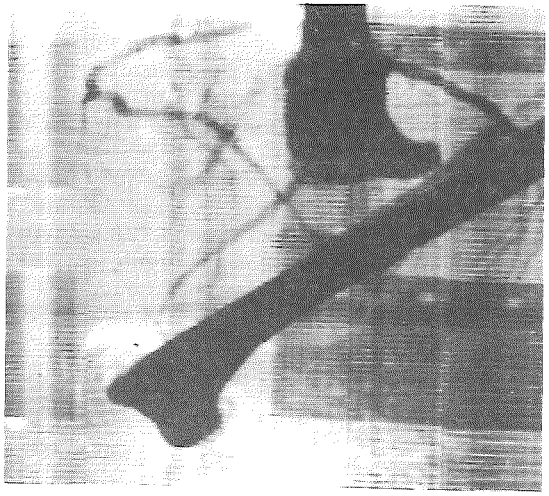

a)

Figure 9. Image of an excised pig heart: taken with a preliminary version of the NIKOS detector system a) above the K-edge, b) below the K-edge (mask), c) subtracted image. 17.4 mg/ml Ba concentration, scan speed 6 cm/s. The upper bone disappears in the subtracted image. The black-white contrast of the second bone indicates that it has moved between the scans of the two images.

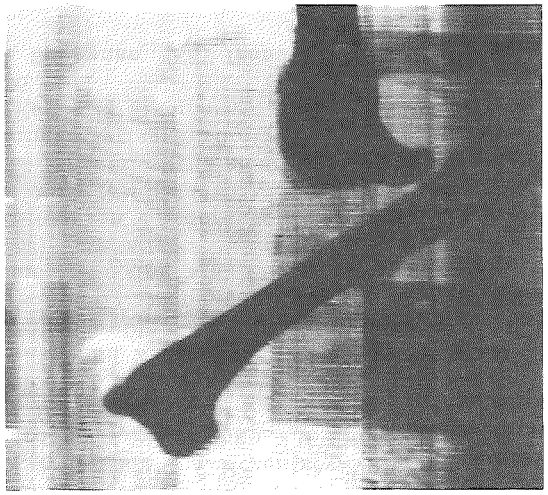

b)

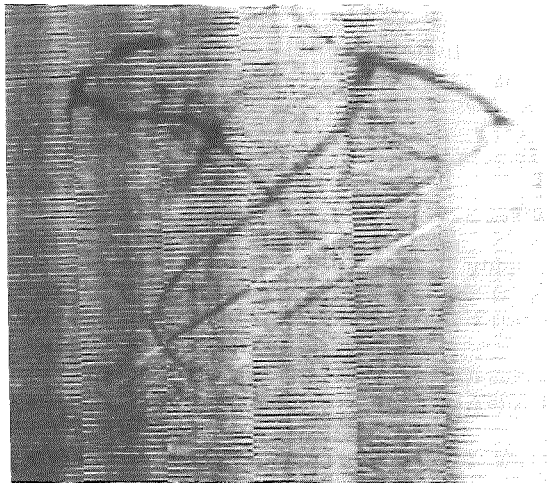

c)

4.0 OUTLOOK

In the near future we will perform additional tests on the individual components of the NIKOS system. These comprise heat load studies of the thin Laue crystals, performance of the fibre optic device and Reticon noise measurements at readout frequencies of up to 1 MHz. Also it is planned to replace the Reticon evaluation circuit by a specially developed electronic readout system that is optimized to our demands. The preliminary version of NIKOS discussed above will be used for our first examination of a living dog.

Next steps then will be the move to an experimental hall where we will have access to a wiggler beam line of sufficient intensity for examinations of humans. This experimental hall is currently under construction and the wiggler installation is planned for 1986/87.

Acknowledgements. We like to thank Dr. M. Pfeiler (Siemens, Erlangen) for providing us with the detector system for more than a year. Dr. Mishima, on leave from Osaka University, helped with the preparation of the pig hearts. M. Dalladas (UKE) did a lot of electronic engineering. Members of the DESY group F58 developed special PADAC modules. The support of the DESY workshops, of the technical staff of Hasylab, especially D. Michael, is gratefully acknowledged. Finally we gratefully appreciate the encouraging support for this work from the DESY directors and from the management of Hasylab.

REFERENCES.

[1] C.A. Mistretta (ed.): Digital Subtraction Arteriography. Year Book Medical Publishers, Chicago (1982).

[2] H.V. Lemke, M.L. Rhodes, C.C. Jaffee, R. Felix (eds.): Computer Assisted Radiology. Proceedings of the International Symposium CAR'85, Springer-Verlag, Berlin (1985).

[3] D. Sashin, E.J. Sternglass, B.S. Slasky, K.M. Bron, J.M. Herron, W.H. Kennedy, L. Shabason, J.W. Boyer, A.E. Pollitt, R.E. Latchaw, B.R. Girdany, R.W. Simpson: SPIE Vol. 347 Application of Optical Instrumentation in Medicine X (1982) 286.

[4] K.H. Höhne, U. Obermöller, M. Riemer: IEEE Transactions on Medical Imaging 3 (1984) 62.

[5] T.L. Houk, R.A. Kruger, C.A. Mistretta, S.J. Riederer, C.G. Shaw, J.G. Lancaster: Investig. Radiol. 14 (1979), 270.

[6] E.B. Hughes, H.D. Zeman, L.E. Campbell, R. Hofstadter, U. Meyer-Berkhout, J.N. Otis, J. Rolfe, J.P. Stone, S. Wilson, E. Rubenstein, D.C. Harrison, R.S. Kernoff, A.C. Thompson, G.S. Brown: NIM 208 (1983), 665.

[7] E.B. Hughes, R. Hofstadter, J.N. Otis, H.D. Zeman, M. Buchbinder, D.C. Harrison, E. Rubenstein, A.C. Thompson, G.S. Brown: these proceedings.

[8] A. Akisada, M. Ando, K. Hyodo, S. Hasegawa, K. Konishi, K. Nishimura, A. Maruhashi, F. Toyofuku, A. Suwa, E. Takenaka : these proceedings.

[9] G.N. Kulipanov, N.A. Mezentsev, V.F. Pindurin, A.N. Skrinsky, M.A. Sheromov, A.P. Ogirenko, V.M. Omigov : NIM 208 (1983) 677.

[10] E.N. Dementyev, E.Ya. Dovga, G.N. Kulipanov, A.S. Medvedko , N.A. Mezentsev, V.F. Pindyurin, A.S. Sokolov, M.A. Sheromov, V.A. Ushakov, E.I. Zagorodnikov: these proceedings.

[11] K. Engelke : Diploma thesis, University of Hamburg, (1984).

[12] M. Böhm, G.C. Nicolae, K.H. Höhne : Proceedings 1st Int. Symp. on Medical Imaging and Image Interpretation, Berlin, IEEE Publ. (1982) 386 - 391.

[13] L.T. Niklason, J.A. Sorenson, J.A. Nelson : Med. Phys. 8 (1981) 677.

[14] D.M. Mills: NIM 208 (1983), 355.

[15] Z.G. Pinsker: Dynamical Scattering of X-Rays in Crystals, Springer-Verlag, Berlin (1978).

[16] T. Kano, K. Kinameri, S. Seki : J. Electrochem. Soc. 129 (1982) 2296.

[17] R.A. Buchanan : IEEE Trans. NS-19 (1972) 81.